J Nanostruct 13(3): 796-805, Summer 2023

RESEARCH PAPER

Therapeutic Effect of Biosynthesis of Selenium Nanoparticles on Enhancing Apoptosis Induction and Cell Lines Arrest in MCF-7 Breast Cancer Cell Lines

*Thifaf Jassim Mohammed [1] * and Majed Kazem Abboud Al-Shibly [2]*

[1] *College of biotechnology, University of Al-Qadisiyah, Iraq*

[2] *College of education, University of Al-Qadisiyah, Iraq*

ARTICLE INFO

Article History:
Received 04 March 2023
Accepted 19 May 2023
Published 01 July 2023

Keywords:
Anticancer activity
Bioengineered nanoparticles
Breast cancer
Cytotoxicity assay
Nanomaterial synthesis
Selenium nanoparticles

ABSTRACT

Samples were collected from Al-Diwaniyah Teaching Hospital in Al-Diwaniyah Governorate - Iraq , period from April 1, 2023 to June 1, 2023. Bacterial samples were collected from wounds and burns, then they were diagnosed using (Vitek-2 compact system- Biomerieux-France), then all the collected bacterial species were tested to produce selenium nanoparticles and the best bacteria capable of producing them were selected. Subsequent steps included characterization of nanoparticles using advanced techniques (Atomic Force Microscopy (AFM), Fourier Transform Infrared Microscopy (FTIR), Microscopy (FESEM) X-ray Diffraction (XRD), and UV-visible spectrophotometry. After successful characterization of the nanoparticles, their biological efficacy and toxicological effects were evaluated. The synthesis process involved incubation, centrifugation, and purification. The anticancer activity of SeNPs was evaluated using the MCF-7 cell line. Cytotoxicity was assessed through the MTT cell viability assay. The AFM measured sizes (10.00 x 10.00 µm, 3.054 x 3.054 µm, 1.135 x 1.135 µm) and showed the surface roughness. FTIR showed peaks at 3749.10, 3454.98, 2926.67, 23 71.95, 632.69, and 451.77 cm^{-1}, indicating vibrations of the functional group. The FESEM results indicated spherical structures and irregular shapes. XRD data revealed the diffraction of the crystal lattice. The intensity indicated a high degree of crystallinity, and UV-visible spectrophotometry showed maximum absorption at 310 nm (0.70). SeNP-treated cells exhibited remarkable growth inhibition rates, with percentages ranging from 38.1% at the lowest concentration (6.25 µg/ml) to an impressive 89.3% at the highest concentration (100 µg/ml). Statistical analysis confirmed the significance of these differences(LCD= 1.091). The investigation into the anti-cancer activity of selenium nanoparticles (SeNPs) against breast cancer cells MCS.7, as detailed in Table 1, provides valuable insights into their inhibitory effects. The concentration-dependent response is evident, with increasing concentrations of SeNPs correlating with higher inhibitory percentages. At the lowest concentration of 6.25 µg/ml, a modest inhibition rate of 38.1±0.12% is observed, which significantly escalates to 89.3±1.13% at the highest concentration of 100 µg/ml. The statistical significance, as indicated by the LSD value of least significant difference (1.091). The current study concluded that SeNPs have the ability to inhibit the spread of cancer and that it is dose dependent, as the inhibition increases with increasing dose and the effect is selective for cancer cells without affecting healthy cells, indicating the potential benefit of SNPs in inhibiting cancer.

How to cite this article
Dehghankelishadi P, Dorkoosh FA. Therapeutic Effect of Biosynthesis of Selenium Nanoparticles on Enhancing Apoptosis Induction and Cell Lines Arrest in MCF-7 Breast Cancer Cell Lines. J Nanostruct, 2023; 13(3):796-805. DOI: 10.22052/JNS.2023.03.020

* *Corresponding Author Email: hifaf.jassim@qu.edu.iq*

INTRODUCTION

In recent decades, the rise of proliferation of cancerous tumors have emerged as critical global health challenge, necessitating innovative approaches to address these pressing issues. The Center of Disease Control (CDC) estimates that cancer cause 10 million deaths annually [1]. Chemotherapy, while effective, often results in severe side effects due to its indiscriminate impact on both healthy and cancerous cells [2]. The burgeoning field of nanomedicine holds great promise for addressing the challenges posed by cancer. Nanoparticles, in particular, offer a versatile platform for drug delivery, imaging, and therapy. Their size and surface characteristics can be precisely tailored to interact with specific cellular targets, enhancing the therapeutic efficacy while minimizing collateral damage to healthy tissues [3].

Selenium, a trace element found in soil, water, and certain foods, has garnered significant attention in recent years due to its well-established antioxidant properties. As an essential micronutrient for various living organisms, selenium plays a crucial role in maintaining cellular function and protecting against oxidative stress [4]. The therapeutic potential of selenium extends beyond its antioxidant capabilities. Research has shown that selenium exhibits anti-inflammatory, immunomodulatory, and anti-cancer properties. Selenium compounds have been investigated for their ability to induce apoptosis (programmed cell death) in cancer cells, inhibit angiogenesis, and modulate the immune response to suppress tumor growth. Moreover, selenium's role in supporting DNA repair mechanisms further underscores its importance in preventing and mitigating the progression of various diseases, including cancer [5].

In nature, Se occurs in four oxidation states: Se6+ (selenate), Se^{4+} (selenite), Se^{2-} (selenide), and Se^{0} (elemental Se). The biological and toxicological effects of Se, whether in anthropogenic or natural environments, depend on a specific chemical state. The zero-oxidation state of Se (Se^{0}) found in selenium nanoparticles (SeNPs) shows lower toxicity and admirable bioavailability compared to other oxidation states of Se^{6+}, Se^{4+} and Se^{2-}. However, biogenic SeNPs have been shown to be safe. So, the biogenic SeNPs are gaining interest and recent experiments have shown that they are better than synthetic SeNPs and even the other organic and inorganic Se species used in the past [6].

This study aims to biosynthesise selenium nanoparticles and the possibility of using them as an alternative treatment for breast cancer.

MATERIALS AND METHODS

Sample collection

Samples were collected from Al-Diwaniyah Teaching Hospital in Al-Diwaniyah Governorate - Iraq, period from April 1, 2023 to June 1, 2023. Bacterial samples were collected from wounds and burns, then they were diagnosed using (Vitek-2 compact system- Biomerieux-France), then all the collected bacterial species were tested to produce selenium nanoparticles and the best bacteria capable of producing them were selected.

Synthesis of nanoparticles

After collecting disease samples randomly,

A B C

Fig. 1. Nanomaterial synthesis process. A: Synthesis using four types of microorganisms to choose the best for production. B: Before preparation. C: After preparation.

growing them, and diagnosing them, dilutions were prepared by mixing 10 ml of the sample with 100 cubic centimeters of normal salin, where a bacterial suspension of the cultivated colonies was made and placed in a tube. The tube was incubated for 24 h at 37°C. The tube was centrifuged at 10,000 rpm for 10 minutes. 10 cc of bacterial filtrate was mixed with 5 mM selenium salts, paying close attention to monitor the resulting color change. With a control tube containing only the bacterial filtrate, both tubes (the negative control and the filtrate mixed with selenium salts) were incubated at a temperature of 30°C for 24 hours. A color shift from yellow to walnut color was observed, indicating the formation of nanomaterials. Purification of the nanomaterial was carried out using a centrifuge at 10,000 rpm for 5 min, with the process repeated to obtain purity. The tubes were placed in the dark to prevent light reaction [7] As in Fig. 1.

Characterization of SeNPs

UV-vis Spectra Analysis

The UV/vis spectrophotometer (200 800 nm) was operated at a resolution of one nm, and it was deemed a straightforward approach for obtaining information about particle concentration, size (diameter), and particle shape shift of the absorbance relay by measuring the absorbance shift [8].

Atomic Force Microscopy Analysis

The spm-AA300 from Angstrom Advanced Inc was used to define the topological surface of the SeNPs. This is accomplished by imaging the three-dimensional shape (topography) of a high-resolution sample surface using the reaction force imposed on it by the sample between the probe and the forces. Controlling the forces between the tip and sample may be accomplished by changing the sample parameters in a predictable manner [9].

FT-IR analysis

The description of functional groups present on the surface of Au NPs and aloe vera extract was examined using FTIR. The spectra were scanned at 4 cm^{-1} resolution, ranging from 4000-400 cm^{-1}. Samples were prepared by dispersing SeNPs in a dry KBr matrix and compessing them into nearly transparent disks. KBr served as a reference standard during sample analysis [10].

X-ray Diffraction XRD

The X-ray diffraction (XRD) pattern of the Ag and Au NPs was determined using an X'Pert PRO analytical X-ray diffractometer operating at a voltage of 45 kV with a current of 40 mA with Cu K radiation using the X'Pert Highscore Plus software to determine the crystal structure. This test was performed in accordance with [11].

FESEM

Visualization of the nanoparticle's form and size was accomplished using a SEM (Scanning electron microscope). Preparation of slides was accomplished by putting tiny drops of nanoparticle suspension on the slides and allowing them to dry. Following the procedure, the slide was subjected to scanning electron microscopy (SEM) (JEOL-MODEL 6390 machine). The microscope was operated at varied magnifications with a speed up voltage ranging from 5 to 10 kV, with a low vacuum, a spot size of 4, and working distances ranging from 5 to 10 mm. This test is carried out in accordance with[12].

Preparation of cancer cells

The MCF-7 cell line was provided by the Iraqi Center for Cancer and Medical Genetic Research at Al-Mustansiriya University. It was preserved in deep freeze at -80° C in RPMI-1640 medium. The cancer cells were activated using special dishes and a special medium was used to grow these cells, which is medium. Dulbecco's Modified Eagle Medium (DMEM) with the addition of 10% of blood serum derived from bovine embryos, as well as the addition of 100 µg/ml of anti- penicillin, and 100 µg/ml of anti- streptomycin, the cells were incubated under anaerobic conditions at 37°C, as it was observed the color of the medium changes from pink to light orange as a result of changing the pH of the medium due to the resulting cellular growth. Upon microscopic examination of the cells, the live cells appear adhered to the wall of the cell growth dish while the dead cells float. The cells are then subjected to centrifugation under very sterile conditions, where the filtrate is discarded and the sediment is taken. The Trypsin-EDTA enzyme was also used for the purpose of uprooting living cancer cells stuck to the walls of the slide for growing cancer cells. This enzyme also works to stop the growth of the transplanted cells when the growth rate reaches 80%, and this percentage is defined by the closeness of the

spaces between the cells, and after that the cells were incubated at 37° C again. This experiment was performed according to [7].

Measurement of cytotoxicity of SeNps

Cytotoxicity assay of SeNps was performed to determine the toxic effect of nanoparticles toward cancer cells. Methyl Thiazolyl Tetrazolium (MTT) cell viability assay was performed using a well-drilled plate, where cell lines were seeded at 1 x 4 10 cells per hole after performing cell counting. It was incubated at 37 °C in an incubator providing anaerobic conditions (50% - CO 2 through the use of containers and bottles equipped with CO 2 during incubation and providing 95% relative humidity by adding water to the peripheral holes in the culture plate, for 24 hours. It was done Obtaining a confluent monolayer of cells with a growth rate of 80%. The cells were treated with the nanoparticle suspension at the following concentrations: µg/ml (6.25 - 12.5 - 25 - 50 - 100). The percentage of cell death was measured 72 hours after being exposed to the nanoparticle suspension, by removing The medium was added and 28 micrograms of MTT dye were added. The cells were incubated for 2.5 hours at 37 ° C after removing the MTT solution. They were incubated in the shaking incubator at 37 °C for 15 minutes. The plate was transferred to the ELISA device to read the results, as the absorbance on the plate reader was at 492 nm. The assay was performed in three replicates for each concentration, and the cell growth inhibition rate (percentage of cytotoxicity) was calculated by the following equation:

$$\text{Cytotoxicity} = \text{AB}/\text{A} * 100$$

Where: A is the control optical density, B is the optical density of the samples.

After that, the shape of the cells was revealed and the growth rate was estimated using an inverted microscope. 200 ml of the cell suspension was taken and placed in a 96-hole plate to accurately calibrate the cells at a density of 1 x 4 (10 cells per ml^{-1}), then incubated for 48 hours at 37 °C. The medium was removed and the tested components were added at (IC50). After the exposure time, the plates were stained with 50 µl crystal violet and incubated at 37 °C for 15 min, and the stain was gently washed with tap water until the dye was removed. The cells were observed under an inverted 40X magnification microscope.

Staining Acridine orange–Ethidium bromide (AO/EtBr) dual

MCF-7 cell line was performed using (AO/EtBr) double staining method, cells were cultured in 96-well plates, cells were treated with nanoparticle suspension and incubated for 24 h. The cells were washed twice with double phosphate buffered saline (PBS), and fluorescent dyes (10 ml) were added to the cells in equal volumes. After incubation times of 15–30 min, cover slides were transferred to view under a fluorescence microscope and magnification was performed at 40X, performed in three replicates for each.

Statistical analysis

All data were analyzed using SPSS software (V.28 Inc., Chicago, USA). and Kolmogorov-Smirnov test of distribution of variables. Usually, the numerical variables distributed between the treated groups were compared using a two-way ANOVA test (univariate and multivariate analysis so that the variance was obtained for the least significant difference (LSD), and all data were expressed as a standard deviation (mean ± SD) and the significance of the differences was discovered when $p < 0.05$ This experiment was conducted according to [7].

RESULTS AND DISCUSSION

Atomic Force Microscopy (AFM)

The characterization of selenium nanoparticles (SeNPs) through Atomic Force Microscopy (AFM) reveals critical insights into their physical attributes at the nanoscale. As shown in Fig. 2A and B, SeNPs exhibit a physical size of 10.00 x 10.00 µm, with an average value of -78.13. The surface roughness is characterized by an average roughness (Ra) of 37.66 mm, a root mean square roughness (Rq) of 61.63 mm, and roughness (Rt) of 607.7 nm. These parameters collectively describe the size and topographical variations across the nanoparticle surface.

Moving to Fig. 2C and D, the physical size is measured at 3.054 x 3.054 µm. Notably, the average value is negative at -4.185, suggesting a specific orientation or feature of the SeNPs. The roughness parameters include an Ra of 1.891 mm, an Rq of 2.745 nm, and an Rt of 42.64 nm, providing detailed information on the surface texture and variations.

Fig. 2E and F, the SeNPs exhibit a physical size of 1.135 × 1.135 µm. The average value is extremely close to zero, indicating a highly uniform structure. The roughness parameters include an Ra of 1.561 nm, an Rq of 2.083 nm, and an Rt of 20.61 nm, emphasizing the fine-scale details and smoothness of the nanoparticle surface. These AFM characterizations play a crucial role in understanding the physical features of SeNPs. The precise measurements of size and surface roughness are vital for comprehending the potential applications of SeNPs, particularly in fields such as medicine and materials science, where their nanoscale properties can be harnessed for various purposes.

Fourier Transform Infrared (FTIR)

Characterization of selenium nanoparticles (SeNPs) using FTIR (Fourier Transform Infrared) spectroscopy spectrum was shown in Fig. 3. The x-axis likely represents the wavenumber in cm^{-1}, which is a unit used in FTIR spectroscopy to denote the frequency of the infrared radiation. The y-axis represents the transmittance percentage, indicating how much of the infrared radiation passes through the sample. Wavenumber ranges from approximately 4000 cm^{-1} to 500 cm^{-1}. Transmittance values vary between 95% and 80%.

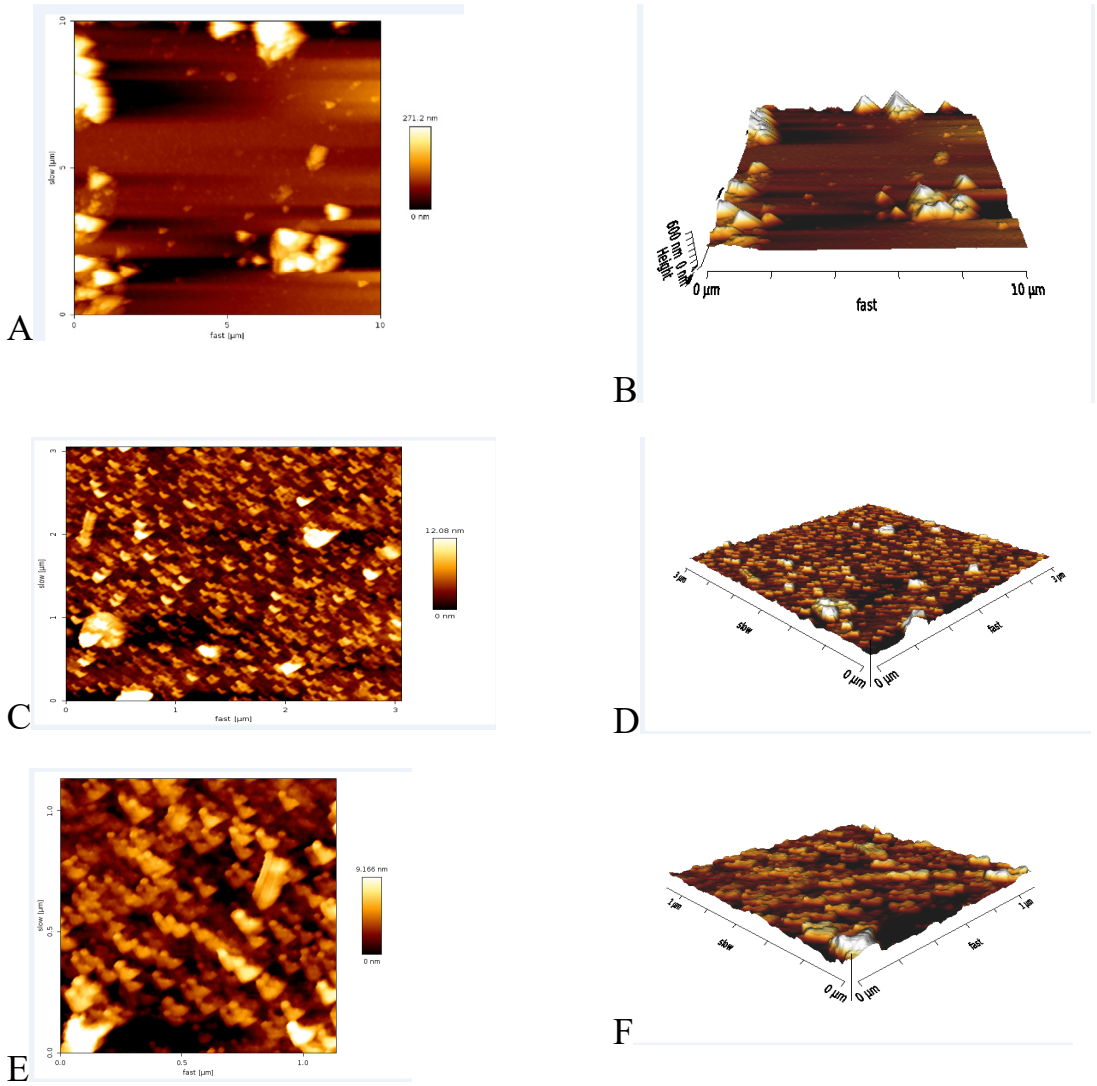

Fig. 2 characterization of selenium nanoparticles (SeNPs) using Atomic Force Microscopy (AFM). A and B:Physical Size: 10.00 x 10.00 µm. C and D:Physical Size: 3.054 x 3.054 µm. E and F:Physical Size: 1.135 × 1.135 µm.

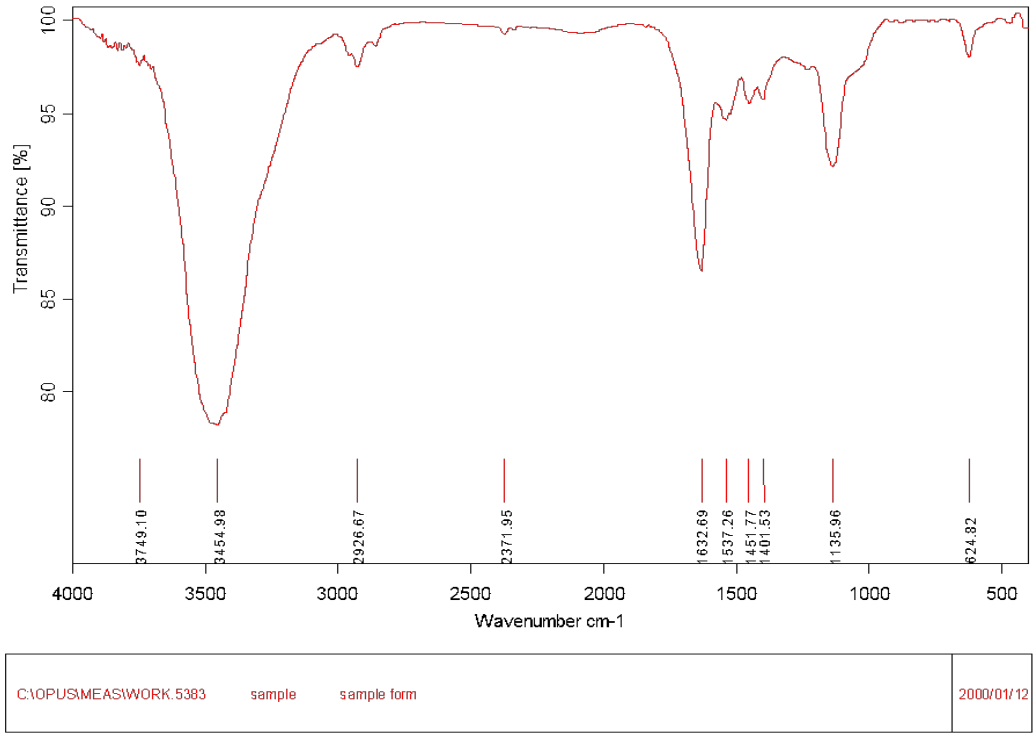

Fig. 3. Characterization of selenium nanoparticles (SeNPs) using FTIR (Fourier Transform Infrared) spectroscopy spectrum.

Prominent peaks are observed around 3749.10 cm^{-1}, 3454.98 cm^{-1}, 2926.67 cm^{-1}, 2371.95 cm^{-1}, 632.69 cm^{-1}, and 451.77 cm^{-1}.

The peaks and troughs in the spectrum are associated with the vibrational modes of different functional groups in the sample. Interpreting specific peaks requires reference to a spectral database or knowledge of characteristic absorption bands for various chemical bonds. Peaks around 3749.10 cm^{-1} and 3454.98 cm^{-1}, for example, may be associated with O-H (hydroxyl) stretching vibrations, while peaks around 2926.67 cm^{-1} could be related to C-H stretching vibrations.

Field Emission Scanning Electron Microscopy (FESEM)

The results of the FESEM (Field Emission Scanning Electron Microscopy) examination conducted at various dimensions (1, 10, 100, 200, and 500 micrometers) revealed distinct morphologies, as illustrated in Figs. 4A to F. At the 1-micrometer dimension, the observed morphology exhibited a spherical shape. This is indicative of a compact and rounded structure, resembling a sphere. At the 10-micrometer dimension, the morphology took on a pattern resembling rough texture. The surface appeared irregular and uneven, suggesting a more complex and textured structure. At the 100-micrometer dimension, the morphology exhibited a somewhat irregular shape, possibly closer to cylindrical. The irregularities in shape suggest a less uniform structure compared to the smaller dimensions. At the 200-micrometer dimension, the morphology displayed spherical and ovoid shapes closely packed together. This suggests a cohesive arrangement with interactions between the spherical and ovoid structures. At the 500-micrometer dimension, the morphology revealed cohesive structures with both ovoid and spherical shapes. Additionally, there appeared to be an intermediate material connecting these shapes, forming a cohesive network. Figs. 4E and F illustrate the spherical and ovoid structures with an intermediate substance between them.

X-ray diffraction (XRD)

The X-ray diffraction (XRD) data was obtained as shown in Fig. 5, and analysis was conducted on the

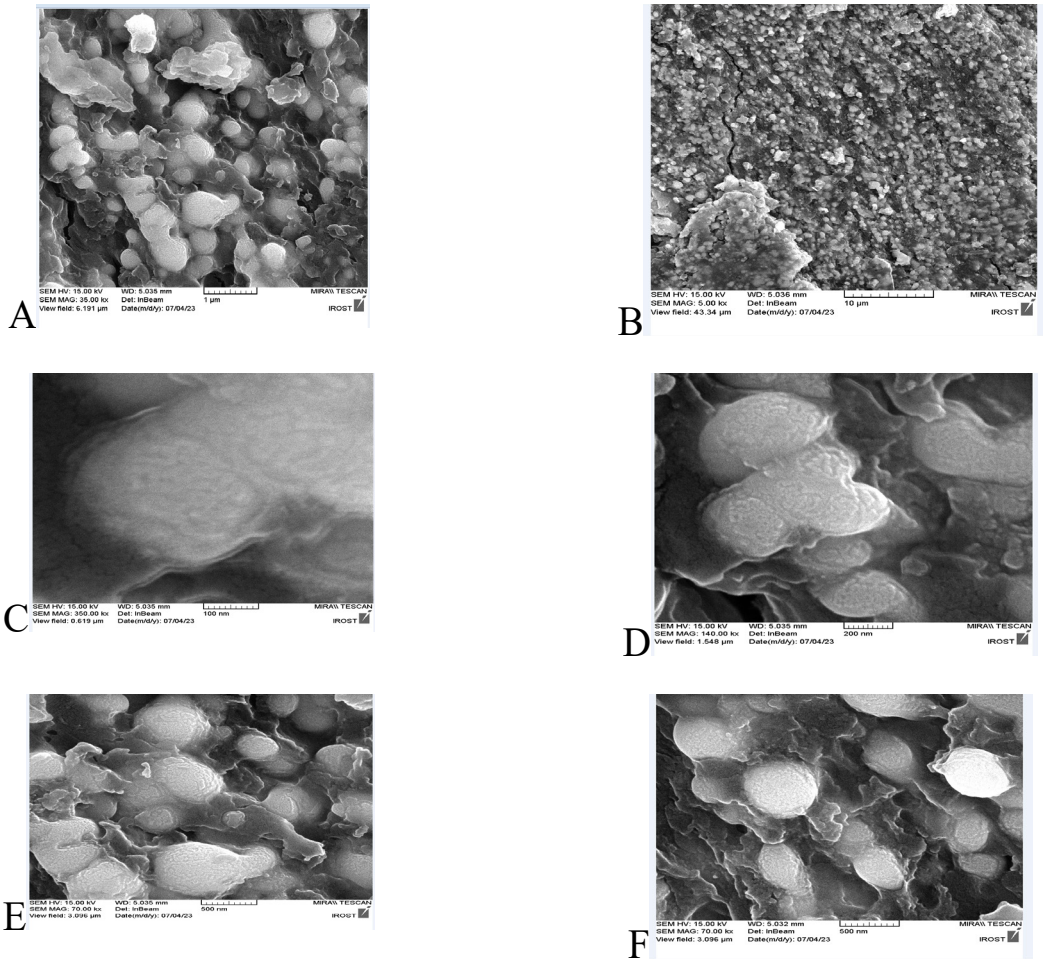

Fig. 4. characterization of selenium nanoparticles (SeNPs) using Atomic Force Microscopy (AFM). A and B:Physical Size: 10.00 x 10.00 µm. C and D:Physical Size: 3.054 x 3.054 µm. E and F:Physical Size: 1.135 × 1.135 µm.

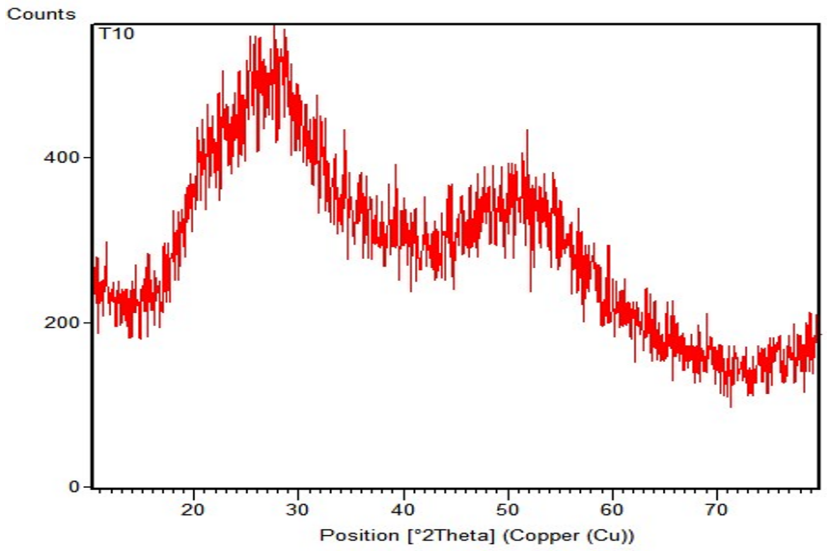

Fig. 5. The X-ray diffraction (XRD) .

resulting diffraction pattern. Peaks were identified in the data, representing the diffraction of X-rays by crystal lattice planes. Peak positions, ranging from 96.6 to 5562.8, were observed and noted.

UV-visible spectrophotometry

The capacity of SeNPs to absorb light in the visible region owing to the Plasmon surface resonance phenomenon was tested, and then the optical absorption was scanned with a wavelength between 200 and 900 nm using a UV-visible spectrophotometer. After 24 hours, UV-visible absorption spectrometry displayed many absorption peaks at certain wavelengths (Fig. 6). The maximum absorbance was observed 0.70 in wavelength 310 nm.

Toxicity of SeNPS

Table 1 details the impact of varying concentrations of selenium nanoparticles on breast cancer cells MCS.7, shedding light on their inhibitory effects. At the lowest concentration tested (6.25 µg/ml), the nanoparticles demonstrated a modest inhibition rate of 38.1±0.12%. As the concentration doubled to 12.5 µg/ml, a substantial increase in inhibition was observed, reaching 59±1.21%. The trend continued, with percentages rising to 71.7±1.03% at 25 µg/ml and a notable 81.5±0.64% at 50 µg/ml. The highest concentration (100 µg/ml) exhibited a remarkable inhibitory effect, boasting a percentage of inhibition at 89.3±1.13%. The LSD value of least significant difference (1.091) underscores the statistical significance of the observed differences between concentrations, suggesting a dose-dependent relationship.

The investigation into the anti-cancer activity of selenium nanoparticles (SeNPs) against breast cancer cells MCS.7, as detailed in Table 1, provides valuable insights into their inhibitory effects. The concentration-dependent response is evident, with increasing concentrations of SeNPs correlating with higher inhibitory percentages. At the lowest concentration of 6.25 µg/ml, a modest inhibition rate of 38.1±0.12% is observed, which significantly escalates to 89.3±1.13% at the

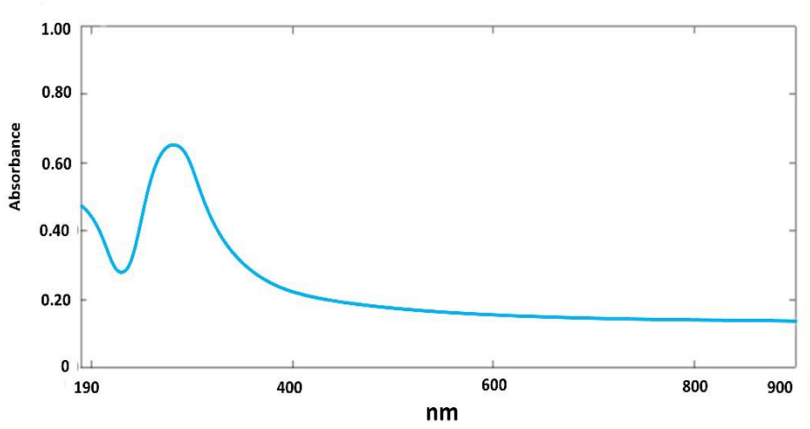

Fig. 6. UV-visible spectrophotometry assay.

Table 1 Effectiveness of different concentrations of selenium nanoparticles against breast cancer cells MCS.7

Nanoscale selenium concentrations (µg/ml)	Percentage of inhibition
6.25	38.1±0.12
12.5	59±1.21
25	71.7±1.03
50	81.5±0.64
100	89.3±1.13
LSD value of least significant difference	1.091

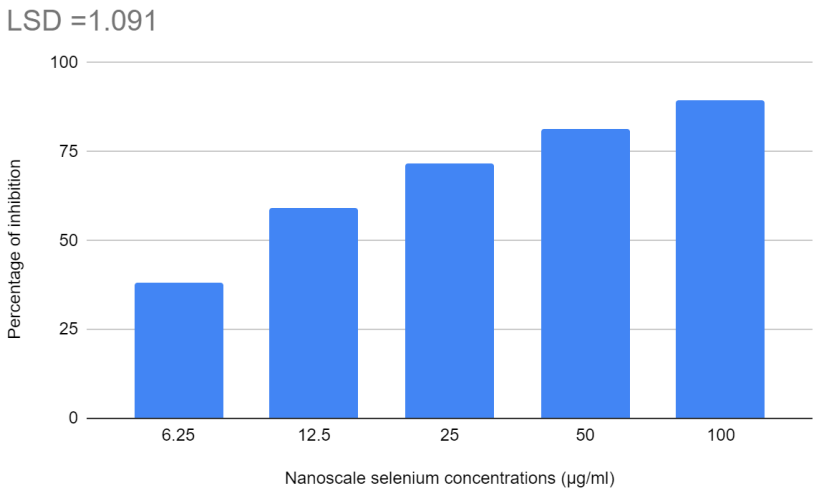

Fig. 7. Anticancer effect of SeNPS

highest concentration of 100 µg/ml. The statistical significance, as indicated by the LSD value of least significant difference (1.091), underscores the dose-dependent relationship and suggests the potential utility of SeNPs in cancer inhibition.

Comparisons with previous studies further highlight the promising anti-cancer properties of SeNPs.[13] synthesized SeNPs using cell suspension and total cell protein of Acinetobacter sp. SW30, comparing their anticancer activity with chemically synthesized SeNPs. While chemically synthesized SeNPs exhibited more significant anticancer activity, they were also toxic to noncancer cells. In contrast, bioengineered SeNPs by Acinetobacter sp. SW30 demonstrated selectivity against breast cancer cells, presenting them as a favorable option for anticancer agents.

Another study by [14] explored the preparation of SeNPs using Bacillus coagulans and investigated their anti-breast cancer activity. The bioengineered SeNPs showed high stability, with an average particle size of 24–40 nm and a zeta potential of –16.1 mV. The cytotoxicity results demonstrated a concentration-dependent effect against MCF-7 breast cancer cells, with an IC50 value of 17.56 µg/mL for SeNPs. Additionally, SeNPs exhibited enhanced apoptotic potential in MCF-7 cancer cells, upregulating pro-apoptotic genes and downregulating anti-apoptotic and pro-cancer genes.

CONCLUSION

In conclusion, the evaluation of anti-cancer activity reveals the potential of selenium nanoparticles in inhibiting breast cancer cells. The dose-dependent relationship observed in the inhibition percentages emphasizes their promising role in cancer treatment. Furthermore, the selectivity and enhanced apoptotic potential demonstrated in bioengineered SeNPs suggest their potential as effective and targeted anticancer agents, though further clinical validation is essential for practical application.

CONFLICT OF INTEREST

The authors declare that there is no conflict of interests regarding the publication of this manuscript.

REFERENCES

1. Murray CJL, Ikuta KS, Sharara F, Swetschinski L, Robles Aguilar G, Gray A, et al. Global burden of bacterial antimicrobial resistance in 2019: a systematic analysis. Lancet. 2022;399: 629–655.
2. Aslam B, Wang W, Arshad MI, Khurshid M, Muzammil S, Rasool MH, et al. Antibiotic resistance: a rundown of a global crisis. Infect Drug Resist. 2018;11: 1645–1658.
3. Mamun MM, Sorinolu AJ, Munir M, Vejerano EP. Nanoantibiotics: Functions and Properties at the Nanoscale to Combat Antibiotic Resistance. Front Chem. 2021;9: 687660.
4. Natasha, Shahid M, Niazi NK, Khalid S, Murtaza B, Bibi I, et al. A critical review of selenium biogeochemical behavior in soil-plant system with an inference to human health. Environ Pollut. 2018;234: 915–934.
5. Garbo S, Di Giacomo S, Łażewska D, Honkisz-Orzechowska E, Di Sotto A, Fioravanti R, et al. Selenium-Containing Agents Acting on Cancer—A New Hope? Pharmaceutics. 2022;15: 104.

6. Ullah A, Mu J, Wang F, Chan MWH, Yin X, Liao Y, et al. Biogenic Selenium Nanoparticles and Their Anticancer Effects Pertaining to Probiotic Bacteria-A Review. Antioxidants (Basel). 2022;11. doi:10.3390/antiox11101916
7. Qadhi IA, Al-Shibly MK. Biosynthesis of selenium nanoparticles by Candida albicans and them antimicrobial effects. J Popl Ther Clin Pharmacol. 2023;30: 360–378.
8. Mourdikoudis S, Pallares RM, Thanh NTK. Characterization techniques for nanoparticles: comparison and complementarity upon studying nanoparticle properties. Nanoscale. 2018;10: 12871–12934.
9. Lindley D. Landmarks—Atomic Force Microscope Makes Angstrom-Scale Images. Physics . 2012;5. Available: https://physics.aps.org/articles/v5/106
10. Naseer M, Aslam U, Khalid B, Chen B. Green route to synthesize Zinc Oxide Nanoparticles using leaf extracts of Cassia fistula and Melia azadarach and their antibacterial potential. Sci Rep. 2020;10: 9055.
11. Vijayan SR, Santhiyagu P, Singamuthu M, Kumari Ahila N, Jayaraman R, Ethiraj K. Synthesis and characterization of silver and gold nanoparticles using aqueous extract of seaweed, Turbinaria conoides, and their antimicrofouling activity. ScientificWorldJournal. 2014;2014: 938272.
12. Rajasekar T, Karthika K, Muralitharan G, Maryshamya A, Sabarika S, Anbarasu S, et al. Green synthesis of gold nanoparticles using extracellular metabolites of fish gut microbes and their antimicrobial properties. Braz J Microbiol. 2020;51: 957–967.
13. Wadhwani SA, Gorain M, Banerjee P, Shedbalkar UU, Singh R, Kundu GC, et al. Green synthesis of selenium nanoparticles using Acinetobacter sp. SW30: optimization, characterization and its anticancer activity in breast cancer cells. Int J Nanomedicine. 2017;12: 6841–6855.
14. Khaledizade E, Tafvizi F, Jafari P. Anti-breast cancer activity of biosynthesized selenium nanoparticles using Bacillus coagulans supernatant. J Trace Elem Med Biol. 2023;82: 127357.